

FLOODPLAIN TOPOGRAPHY AND AVULSION PATHFINDING CONTROL STRATIGRAPHIC ARCHITECTURE IN A NUMERICAL MODEL OF A FLUVIAL FAN

CAITLIN SIFUENTES,^{1,2} HARRISON K. MARTIN,^{1,3} KYLE M. STRAUB,⁴ ELIZABETH A. HAJEK,⁵ AND DOUGLAS A. EDMONDS¹

¹*Department of Earth and Atmospheric Sciences, Indiana University, Bloomington, Indiana, U.S.A.*

²*Geosyntec Consultants, Long Beach, California, U.S.A.*

³*Division of Geological and Planetary Sciences, California Institute of Technology, Pasadena, California, U.S.A.*

⁴*Department of Earth and Environmental Sciences, Tulane University, New Orleans, Louisiana, U.S.A.*

⁵*Department of Geosciences, Penn State University, University Park, Pennsylvania, U.S.A.*

ABSTRACT: Buried channel sand bodies are important reservoirs of subsurface water and energy resources, but their arrangement and interconnectedness are difficult to predict. The dominant process that distributes channels and their sediments in alluvial basins is river avulsion, which occurs when a channel seeks a new location on the adjacent floodplain. Floodplain sedimentation, incision, and channel levee growth influence channel pathfinding during avulsion, and should control key aspects of the stratigraphic arrangement of channel bodies, including compensational (spatially and temporally even) deposition, stratigraphic completeness, and facies distributions; however, this impact has been difficult to isolate in natural and experimental basin fills. To test how different avulsion pathfinding parameters influence stratigraphic architecture, we use a numerical model of a fluvial fan to produce synthetic fluvial stratigraphy under seven different runs with progressively more complex channel pathfinding rules. In the simplest models where pathfinding is set by a random walk, the channel rapidly changes position and avulsions spread across the fan surface. The corresponding deposit is dominated by channel facies, is relatively incomplete, and the compensation timescale is short. As rules for pathfinding become more complex and channels can be attracted or repulsed by pre-existing channels, lobe switching emerges. Deposits become more diverse with a mix of channel and floodplain facies, stratigraphic completeness increases, and the compensation timescale lengthens. Previous work suggests that the compensation timescale is related to the burial timescale and relief across the depositional surface, yet we find that compensation approaches the burial timescale only for model runs with high morphodynamic complexity and relatively long topographic memory. Our results imply that in simple systems with limited degrees of freedom, the compensation timescale may become detached from the burial timescale, with uniform sedimentation occurring quickly relative to long burial timescales.

INTRODUCTION

The arrangement, architecture, and stratigraphic stacking patterns of channel sand bodies in alluvial basins have been used to identify changes in allogenic forcings such as eustatic sea-level rise, subsidence, and climate variability (Allen 1978; Bridge and Leeder 1979; Mackey and Bridge 1995). However, many of these initial interpretations have been revisited because the influence of allogenic processes on alluvial architecture is not recognizable at all time and space scales (Hajek and Straub 2017). Previous work has defined a time window or stratigraphic thickness—called the compensational scale—where deposition patterns in a basin transition from stochastic (or variable) to deterministic (or even) (Straub et al. 2009; Wang et al. 2011; Chamberlin and Hajek 2015; Hajek and Straub 2017; Trampush et al. 2017). Stochastic deposition is driven by local autogenic variability in the transport system, whereas deterministic deposition occurs when sedimentation patterns reflect the even and uniform filling of available accommodation (Straub et al. 2009; Wang et al. 2011; Chamberlin et al. 2015; Trampush et al. 2017). The time or length scale at which stochastic (variable) deposition transitions to

deterministic (even) is the compensation timescale and it is estimated through the spatial variability of depositional patterns over a range of time or thickness scales in a basin fill (Sheets et al. 2002; Straub et al. 2009; Wang et al. 2011; Straub and Pyles 2012; Hajek and Straub 2017; Trampush et al. 2017). While the compensational scale has proven to be a useful diagnostic tool for understanding broad controls on facies architecture and stratigraphic completeness, the specific ways depositional processes influence the compensation scale remain unclear. For example, in alluvial basin deposits, processes like alluvial-ridge development, floodplain filling trends, and channel avulsion styles and patterns have been recognized as potentially contributing to different measured compensation scales (see review by Hajek and Straub 2017). Compensation can also be hierarchical, starting at small scales where individual channel beds compensate for older channel beds (Mutti and Sonnino 1981; Straub and Pyles 2012), and extending to higher scales where alluvial ridges or precession-scale floodplain aggradation cycles cause compensation (Wang et al. 2023). However, the specific ways these processes, particularly the movement of channel belts through avulsion, may influence compensation timescales in alluvial basins has been untested.

Over the last 15 years, numerous studies using statistical, geometric, and laboratory models have shown that compensation occurs at a timescale of the local surface relief divided by the long-term aggradation rate (see review by Hajek and Straub 2017). This is the time required for nonuniform (e.g., channelized) sediment distribution networks to migrate across the basin and fill it evenly (Sadler 1993; Straub and Foreman 2018). This can also be thought of as the time required to generate enough relief across the land surface so that channels are attracted into low areas during avulsion, and this may change moving downstream (Gearon et al. 2024). The time required for even basin filling has also been referred to as a burial timescale, because it represents the average time required to bury a particle deeply enough that it will not be re-exhumed or reworked by the largest reasonable erosional event (e.g., scour at the base of a channel avulsion) given the regional long-term sedimentation rate. This timescale was derived from geometric cross-sectional models that have shown that when a critical landscape relief is achieved and newly avulsed channels find the lowest elevation point, then compensation emerges at the burial timescale (Straub et al. 2009; Wang et al. 2011). Similarly, more complex physical and numerical experiments of fan or delta evolution have shown the same behavior (Straub et al. 2015; Li et al. 2016; Salter et al. 2020; Wang et al. 2021; Hariharan et al. 2022), and field studies of ancient deposits have indicated that compensational basin filling requires sufficient durations to bury deposits up to several channel depths in thickness (Wang et al. 2011; Chamberlin et al. 2016). Furthermore, these related concepts of compensation and burial timescales have been shown to be useful estimators of stratigraphic completeness and time preservation in alluvial basins (Foreman and Straub 2017). These efforts all point toward relief generation as a key influence on compensation and stratigraphy of fan or delta systems. Subsequently, the rate of relief generation is important—in fan or delta experiments the addition of mud and cohesiveness decreased channel lateral mobility, generated more relief, and increased the compensation timescale (Li et al. 2017). Similarly, the presence of allogenic forcing can reduce channel mobility and lengthen the compensation time (Wang et al. 2021).

While landscape relief has been shown to correspond to the compensation scale, the specific mechanisms through which topographic relief influences the compensation timescale have not been investigated. This linkage between relief and basin filling most likely arises because surface topography and relief influence channel steering, or pathfinding, during avulsion. Pathfinding is the collective set of processes that govern how an advancing avulsion channel moves across the floodplain before it stabilizes in a new location. For avulsions to evenly fill the basin and create compensational stratigraphy, avulsing channels must preferentially pathfind into topographic lows. If relief generation is broadly distributed over an area, then this may create favorable slopes that steer channels into topographic lows. But relief generation may also occur as long, linear alluvial ridges, which restrict movement of the pathfinding channel and makes parts of the surface inaccessible (Bridge and Leeder 1979; Mackey and Bridge 1995; Karszenberg and Bridge 2008; Reitz et al. 2010; Martin and Edmonds 2022). Additionally, abandoned channels on the surface also have negative relief, which can attract an advancing channel (Reitz et al. 2010; Reitz and Jerolmack 2012; Martin and Edmonds 2022). Over time, the steering of avulsing channels via topography and relief generation at different scales may be a primary influence on compensation and the timescale at which a basin can be observed to fill evenly (Allen 1978; Bridge and Leeder 1979; Mackey and Bridge 1995; Chamberlin et al. 2016).

The degree to which connections between channels and their floodplains facilitate relief generation, steering of avulsion channels toward or away from previously occupied locations, and the emergence of compensation on fans or deltas has not yet been explicitly explored. Recent modeling from Martin and Edmonds (2022, 2023) showed that, on one hand, when abandoned channels repel or block pathfinding channels, active flow is routed into fewer channels and avulsion occurrence is pushed farther downstream as a result. On the other hand, when abandoned channels provide favorable topographic pathways that

attract avulsing channels, avulsion occurrence is pulled farther upstream. Complexity arising from abandoned channels attracting or repelling avulsion channels during pathfinding can create additional levels of process hierarchy on a landscape (Ganti et al. 2020). For example, larger-scale lobe switching arises in models of fluvial fans when channel activity becomes focused on one side of the fan until enough deposition fills accommodation space, lowers the slope, and the channel activity switches to the opposite side of the fan (Martin and Edmonds 2022). The rules governing channel pathfinding during avulsion play a key role in how sediment is routed across an alluvial basin and, consequently, may strongly influence compensation, facies distribution, and stratigraphic completeness in alluvial basins.

To explicitly investigate how avulsion pathfinding influences stratigraphic architecture, we used a new version of a numerical, physically based cellular model (Martin and Edmonds 2022) to build synthetic stratigraphy under different avulsion pathfinding scenarios that varied parameters such as slope dependence and influence of previous channels. This model creates fluvial fans, which are an ideal landform to focus on because they have some of the highest avulsion rates seen in the observational record (Valenza et al. 2020) and are also densely populated with abandoned channels that create topographic relief on the floodplain (Stanistreet and McCarthy 1993; Assine 2005; Leier et al. 2005; Rossetti and Valeriano 2007; Chakraborty et al. 2010; Bernal et al. 2011; Weissmann et al. 2013; Hansford and Plink-Björklund 2020). We conducted a series of seven model runs that build in complexity from the simplest model, where pathfinding is controlled only by a downstream-weighted random walk, to one that includes rules for pathfinding channels to be attracted and repulsed by abandoned channels. We sequentially added complexity to identify how pathfinding processes affect compensation, facies architecture, and completeness.

METHODS

The RiverWalk Model

The RiverWalk Model is a numerical, physically based cellular model that we use to test how different avulsion pathfinding parameters influence stratigraphy (Martin and Edmonds 2022). A full description of the RiverWalk Model is in Martin and Edmonds (2022). In the model, a single channel exits the mountain front and channelized sediment transport, deposition, and erosion are determined via diffusion (Paola et al. 1992). At the upstream boundary, water and sediment enter at a fixed rate of $1.9 \times 10^6 \text{ m}^3 \text{ yr}^{-1}$ (assuming a 100-m-wide channel) and $400 \text{ m}^3 \text{ yr}^{-1}$, respectively, and the initial slope in the domain is 2.5×10^{-3} . Accommodation is generated by subsidence, which decreases linearly into the basin from $1 \times 10^{-5} \text{ m yr}^{-1}$ to $5 \times 10^{-6} \text{ m yr}^{-1}$ at the downstream boundary. To mimic natural fluvial fans, each model runs for 3 Myr with a domain that is 150 km wide and 150 km long. All model runs have a time step of 10 years and spatial discretization of 500 m square cells. All simulations initialize across the floodplain with a uniform slope equal to the equilibrium slope of a straight channel carrying the incoming water and sediment. Then the first channel path is chosen by random walk, and because that path will be longer than a straight channel, the river aggrades and avulses, and the simulation begins.

Following Jerolmack and Paola (2007) the channel is assumed to be subgrid scale. Cells are classified as either active channel, floodplain, or abandoned channel. In each model cell with an active channel, two topographic elevations are recorded: levee height and channel-bed elevation. These elevations are coupled so that channel-bed aggradation causes levee growth. When the channel-bed elevation is the same as an adjacent floodplain cell (i.e., superelevation), then avulsions occur in the model in response to a triggering event. To mimic the stochastic nature of natural triggering events, we fix the average avulsion period to 30 years, meaning that there is a 1/30 chance of an avulsion occurring in any given model year. If a trigger occurs, an avulsion location is randomly selected

from all the superelevated cells. After the avulsion, the channel seeks a new path (the pathfinding phase) determined from a five-direction downstream-weighted random walk.

During the pathfinding phase, abandoned channels on the floodplain can repulse or attract the avulsion channel. Each model run uses a pair of nondimensional parameters to specify how repulsive (α_R) or attractive (α_A) abandoned channels will be. Conceptually, abandoned channels surrounded by tall levees could repel pathfinding avulsion flows. In the model, an abandoned channel is repulsive when:

$$L_h > \alpha_R * h_{avul} \quad (1)$$

where the abandoned-channel levee height (L_h) is greater than some fraction (α_R) of the pathfinding-channel depth (h_{avul}). Levee height is measured as the difference in elevation between the levee height of the abandoned channel and the bed elevation of the approaching pathfinding channel.

If the abandoned channel levees do not repel oncoming avulsion flows, then reoccupation via attraction could occur. Attraction occurs when an abandoned channel is deep enough to capture (or annex) the pathfinding avulsion channel. In the model, an abandoned channel is attractive when:

$$h_{aban} > \alpha_A * \bar{h} \quad (2)$$

where the depth of an abandoned channel cell (h_{aban}) must be greater than some fraction (α_A) of the mean channel depth when it was active (\bar{h}). For example, an abandoned-channel cell in a scenario specifying more-attractive abandoned channels ($\alpha_A = 0.25$) might need to only be 0.25 times its original depth, whereas the same cell in a scenario with less-attractive abandoned channels ($\alpha_A = 4$) might have to be four times its original depth. If the criteria are met, repulsion or capture will automatically occur when the pathfinding channel is adjacent or diagonal to abandoned channel cells. These rules can cause a pathfinding avulsion to become trapped in an internally drained basin, in which case the avulsion fails and the channel returns to its previous location.

In the model, abandoned channels heal through levee erosion and overbank deposition. We assume that the positive relief of the levee is eroded over time and the abandoned-channel bed is aggraded and both occur at the same pace. The rate is constant so that a mean channel depth heals after 55,000 years. When abandoned channels heal to less than 25% of their average initial depth, they no longer influence pathfinding and become floodplain cells.

Floodplain cells are defined as those cells that do not contain the active channel or an abandoned channel. Floodplain deposition in the model is the product of two variables. A base overbank aggradation ($A_{fp,base}$) that increases linearly away from the mountain front to represent progressive higher flux of fine material downstream, and a differential aggradation that is normalized by mean channel depth (\bar{h}). The base aggradation rate is $2.0 \times 10^{-7} \text{ m yr}^{-1}$ at the upstream boundary of the model domain and $5.0 \times 10^{-6} \text{ m yr}^{-1}$ at the downstream boundary. Differential overbank deposition increases linearly with relief between the topographic high and a far-field, unchannelized floodplain cell in the current grid row ($\eta_{high,max} - \eta_{farfield}$). Within each timestep, the instantaneous deposition rate ($A_{fp,base}$) cannot exceed subsidence (σ):

$$A_{fp,tot} = \min \left\{ A_{fp,base} * \frac{\eta_{high,max} - \eta_{farfield}}{\sigma \bar{h}} \right\} \quad (3)$$

The Stratigraphic Model

For this study, we added a stratigraphic component to the RiverWalk model. This component takes as input a series of matrices describing the elevation and cell type (active channel, abandoned channel, or floodplain)

of each cell for each timestep. For output, the component generates the subsurface stratigraphy for any chosen 2-D cross section (along-strike or along-dip). In principle, iterating the component over all rows or columns would create a 3-D volume. However, because changes in elevation between individual timesteps can range from large (meters of erosion during initial incision after an avulsion) to vanishingly small (the difference in subsidence between successive rows is $\sim 10^{-7} \text{ m}$ per timestep), storing all accumulated and eroded sediment data for each timestep of the entire model run would result in impractically dense stratigraphic cross sections. To facilitate well-resolved basin-scale stratigraphic analyses, we choose a vertical cell size of 10 cm, representing the thinnest bed of interest in the basin fill. During each model run, we exported elevation changes through time for all cells in the basin; then the stratigraphic module uses those changes to reconstitute the stratigraphy. In the stratigraphic module whenever the absolute value of elevation change exceeded 10 cm, we modified the stratigraphic cross section by adding or removing stratigraphic cells in 10 cm increments, with the remainder returned to an accumulator matrix. Using an accumulator matrix in this way allowed us to handle both large, instantaneous elevation changes and minuscule differences as they can accumulate over millions of years.

For cells that increased in elevation, the cell type (active channel, abandoned channel, or floodplain) at the time of aggradation was assigned to the new strata as a representative facies. While the model does not resolve grain-size differences, we assume that deposition for each cell type would create different facies: 1) active channels would likely create sand rich channel-fill bodies; 2) abandoned channels would probably create heterogeneous finer-grained fills (Toonen et al. 2012; Moran et al. 2017; Li et al. 2020); and 3) floodplains would record the mud-rich aggradation away from channels.

Experimental Design

We conducted seven model runs to explore how pathfinding influences stratigraphic architecture, as defined by the emergence of compensation, facies distribution, and completeness. These runs were designed to increase in complexity by sequentially adding new processes. The first model is the simplest, where a channel avulses only at the fan apex (if that location is superelevated and a trigger occurs) and avulsion pathfinding is set by a downstream random walk. The downstream cell, and downstream right and left cells, have probabilities of 40%, 20%, and 20% respectively, while the two lateral cells have 10% probabilities. In this model, there is no attraction or repulsion from abandoned channels (random-walk apical, RWA). The second model adds slope dependence to pathfinding (slope-dependent apical, SDA). The five random-walk cells are weighted by their relative bed slopes where the steepest to shallowest paths have 40%, 27.5%, 17.5%, 10%, and 5% likelihoods of selection. The third and fourth runs have the same pathfinding rules as the first and second runs, respectively, but the apical avulsion condition is relaxed and avulsions occur anywhere there is superelevation (random-walk multi-location RWM, and slope-dependent multi-location, SDM). Starting from model SDM, three more runs added only attraction (SDM-A), only repulsion (SDM-R), and both attraction and repulsion (SDM-AR). Model runs RWA, SDA, RWM, and SDM have α_A and α_R set to 1000 to avoid any attraction or repulsion. In SDM-A, $\alpha_A = 0.25$, in SDM-R $\alpha_R = 1$, and in SDM-AR $\alpha_A = 0.25$ and $\alpha_R = 1$. See Martin and Edmonds (2022) for more details on these parameters.

Analysis of Channel Dynamics, Compensation, Completeness, and Stratigraphic Architecture

To measure the evenness of sedimentation across the basin through time and the emergence of compensation, we used the compensation statistic (Straub et al. 2009; Wang et al. 2011; Chamberlin and Hajek 2015;

Trampush et al. 2017). The compensation statistic (σ_{ss}) analyzes the standard deviation of sedimentation relative to subsidence (Straub et al. 2009; Wang et al. 2011; Chamberlin and Hajek 2015; Hajek and Straub 2017; Trampush et al. 2017):

$$\sigma_{ss} = \left(\int_L \left[\frac{r(T;x)}{\hat{r}(x)} - 1 \right]^2 dL \right)^{1/2} \quad (4)$$

σ_{ss} is calculated by dividing the average deposition rate (r) at position x along a strike line during some time interval (T). \hat{r} is the long-term sedimentation or subsidence rate. Because our model runs accumulate sediment beyond what is subsided (i.e., build positive topography as fluvial fans), we use the long-term sedimentation rate. L is the width of the area of interest, which we set to the middle 25 km of the domain (in the along-strike direction) to remove the edge effects from a curved topographic surface. Values of σ_{ss} decrease as a power law as the time window grows, and the slope of this decay is defined as the compensation index (κ). The time window when κ changes and approaches one marks the emergence of compensation and even sedimentation across the basin (Sheets et al. 2002; Straub et al. 2009; Wang et al. 2011; Straub and Pyles 2012; Trampush et al. 2017). Note that the κ value is actually negative but is reported as positive following convention (Straub et al. 2009). We analyzed compensation statistics on stratigraphy recorded from 1 Myr to 3 Myr in the model to avoid spin-up time associated with establishment of the fan and estimated the compensation timescale using a change-point-detection algorithm to identify the timescale where $\kappa < 1$ shifts to $\kappa \sim 1$. The change-point-detection algorithm looks for the intersection of two log-log linear trends (Straub et al. 2023). Here we differentiate the compensation timescale as a measure of statistically even basin filling (Eq. 4; cf. Straub 2009) from estimates of the timescale required to bury maximum topographic relief on a landscape given \hat{r} (cf. Wang et al. 2011) by referring to the latter as the burial timescale.

Variability in channel dynamics is evident in RiverWalk as channels shift from one side of the fan to the other (Martin and Edmonds 2022, 2023). To quantify timescales of channel activity, we used a continuous wavelet transform to evaluate the structure of active-channel location through time and determine the dominant frequency of channel or lobe switching through an entire model run, which is described as

$$\psi_{\lambda,t}(u) \equiv \frac{1}{\sqrt{\lambda}} \psi \left(\frac{u-t}{\lambda} \right) \quad (5)$$

where ($\psi_{\lambda,t}(u)$) is the family of functions or wavelets, u is time, λ is a scale parameter, and t is a location parameter (Kumar and Foufoula-Georgiou 1997). Compared to a Fourier Transform, the continuous wavelet transformation is beneficial since the time series signal changes through time and the scales of switching are not constant. For example, when λ is scaled up, it looks at the long-term trends of the signal, allowing us to see shifts in the dominant switching frequency of our time series (Kumar and Foufoula-Georgiou 1997).

We evaluate stratigraphic completeness to assess how the evenness of basin filling and topographic evolution of the fan surface impact time preservation in the stratigraphic record. Stratigraphic completeness is the fraction of time recorded in the strata relative to the total elapsed time averaged across the middle 25 km of the domain (Sadler 1981; Tipper 1983; Kemp 2012; Straub et al. 2020). The timescale at which a record is considered complete (99% of time elapsed is recorded) has previously been shown to scale with compensation and burial timescales (Straub et al. 2020).

To explore the relationship between the evolution of surface topography and the preservation of alluvial deposits, we evaluate how topographic relief varies across the model surface through time. Relief is calculated across a

strike cross section using a moving-window approach. Moving across the section with a four-cell window, we calculate the relief as the maximum minus the minimum within the window. We then averaged the values across the middle 25 km of the domain through time for each model run. Finally, we autocorrelated this relief through time signal to assess landscape “memory,” or the degree to which surface relief at a given time is inherited from previous timesteps. The autocorrelation function assesses correlation over progressively longer shifts; for example, a white-noise signal has no autocorrelation at any time shift greater than zero.

To compare cross sections of the subsurface from different runs, we normalized distance into the basin by mass extraction following Paola and Martin (2012):

$$\chi(x) = \frac{1}{Q_{s0}} \int_0^x B(x)r(x)dx \quad (6)$$

The chi value (χ) can be described as the downstream distance (x) at which some given fraction of the initial sediment input has been deposited, where r is the net rate of deposition. This equation characterizes fluvial transport systems with varying fan widths (B) and is normalized by the total incoming sediment supply (Q_{s0}). For example, $\chi = 50\%$ corresponds to the location downstream from the fan apex where half of the incoming sediment supply has been deposited. All stratigraphic sections are analyzed at $\chi = 50\%$ where subsidence is high, there is sufficient accommodation to accumulate sediment, and it is far enough from the apex of the fan to not be influenced by the upstream boundary condition. For each stratigraphic section we compare the fraction of the cross section that is channel-fill deposit and qualitatively assess the distribution of channel fill, abandoned channel, and floodplain facies across the fan deposit. Initial exploration showed that the results did not vary significantly over reasonable values of χ .

RESULTS

Stratigraphy and Channel Dynamics

Our model runs show that the different pathfinding rules create deposits that resemble fluvial fans in planform appearance (Fig. 1). Some fans are narrower and more elongate (Parts A–C), whereas others are wider and shorter (Parts D–G). On the wide, short fans there is a downstream transition from the distributive-fan surface to a more tributive zone (see example in Fig. 1D) (Martin and Edmonds 2023). The boundary between the distributive and tributive zones marks the extent of sediment distribution and thus the fan. The channel dynamics and associated stratigraphy at $\chi = 50\%$ show remarkable differences: different pathfinding rules alone can clearly change how the channel migrates over the fan surface (Fig. 2) and the associated stratigraphic architecture (Fig. 3). For model run RWA, the fan is relatively narrow, the channel activity is concentrated near the center, and the dominant stratigraphic facies are channel-fill deposits (Fig. 2A, 3A). The average channel return time, calculated as the average time before a channel returns to a given position across the fan width, is fast at 2.7 kyr (Table 1). The channel-fill fraction across the fan is 0.96 and the average scour depth is 0.46 m (Table 1). The deposit is dominantly channel-fill because the random-walk pathfinding keeps channel activity normally distributed around the middle of the fan, and the short channel return time means that overbank sediment does not accumulate between channel visits to bury older channel deposits and protect them from reworking by relatively deep scours. This happens with minimal pathfinding rules because there are no restrictions on where the channel can go, and channel-fill deposits are able to accumulate everywhere. There are more abandoned-channel facies on the fan margins where the active channel does not visit as often (Fig. 3A). Adding a slope dependence to pathfinding in run SDA increases the fan width over time as

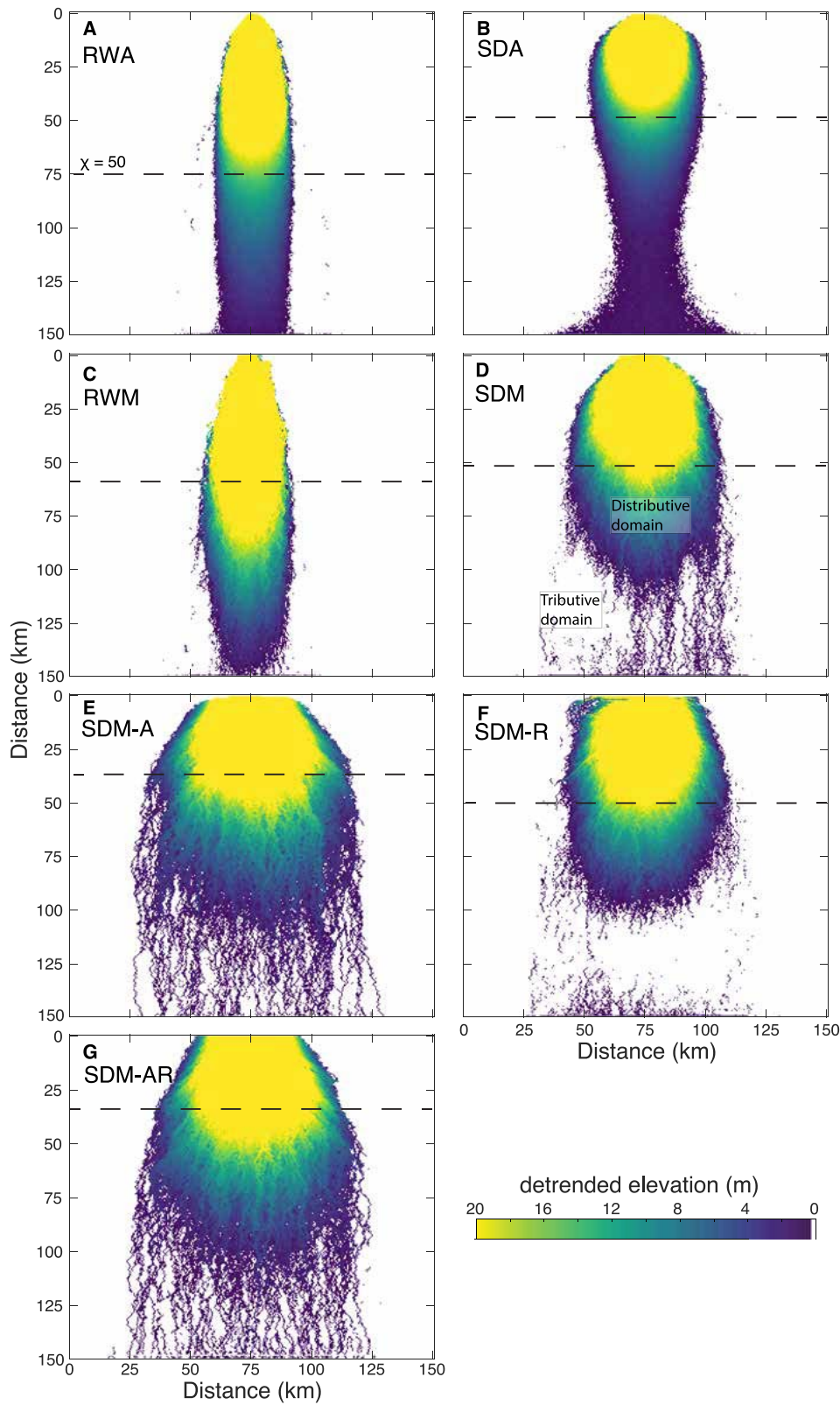


FIG. 1.—**A–G**) Planform morphology of the fan at the end of the model run. Elevation is detrended from the background slope. All elevation colormaps are the same, but the maximum elevation is clipped to 20 m to show variability. Dashed horizontal line shows downstream position where $\chi = 50\%$.

the fan’s lateral side slopes force the channel towards the margins (Fig. 2B). This also reduces the channel return time to 1.79 kyr, but it is still fast compared to other runs. The stratigraphy is similar to that of the RWA experiment, and the channel fraction remains high at 0.99 and the scour depth

is 0.42 m (Table 1; Fig. 3B). In both RWA and SDA, there are virtually no floodplain deposits preserved within the fan (Fig. 3A, B).

Allowing avulsions to occur anywhere on the fan surface in runs RWM and SDM, as opposed to restricting them to the fan apex as in the RWA and

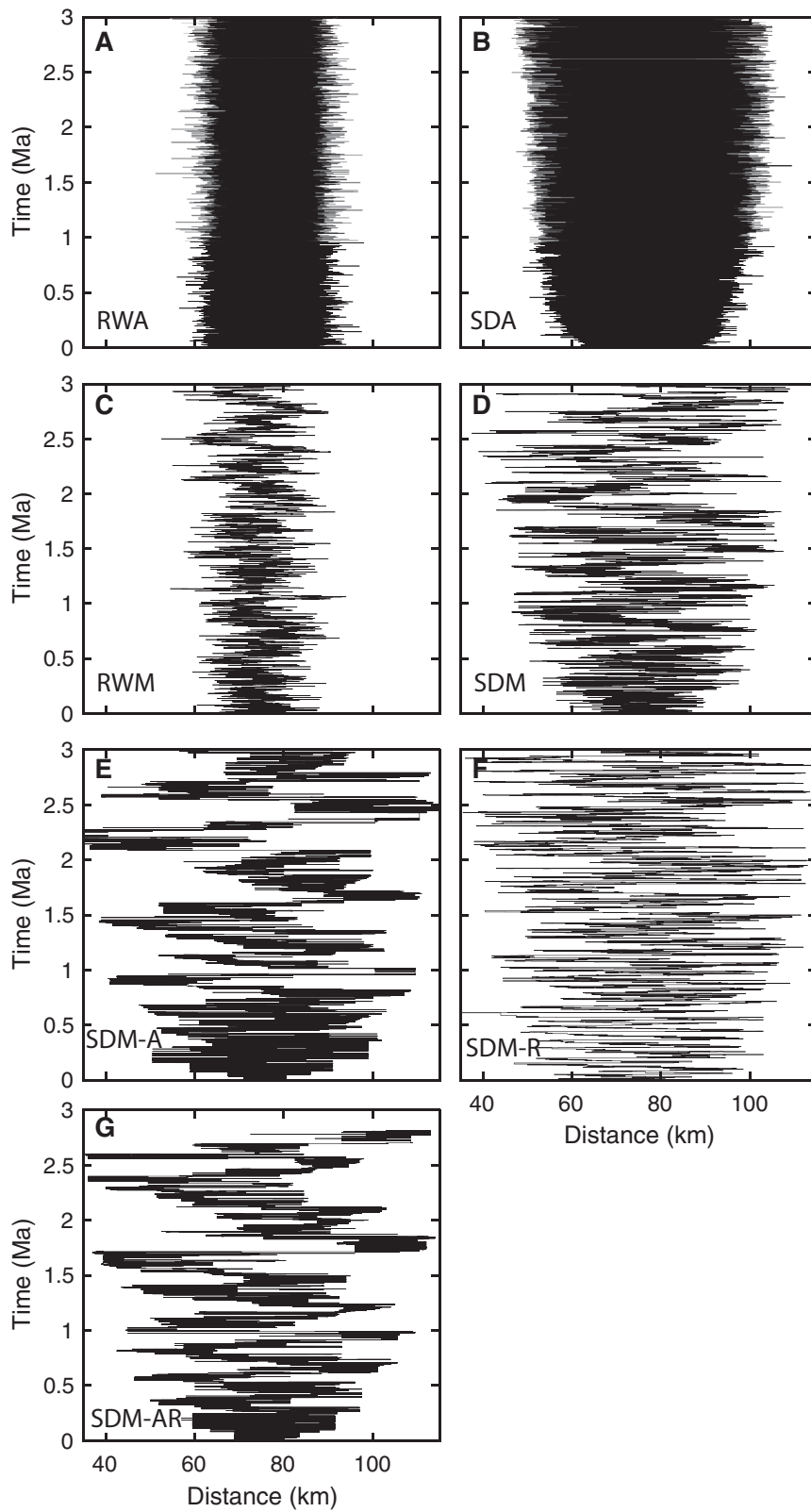


FIG. 2.—**A–G**) Active-channel position over time for the seven model runs at the $\chi = 50\%$ cross section. The model domain is actually 150 km wide, but the distance is cropped to the width of channel activity.

SDA runs, significantly changes channel dynamics. Channel activity starts to oscillate from one side of the fan to the other (Fig. 2C, D), as channel return time increases substantially to ~ 50 kyr (Table 1). This occurs because nodal avulsions that switch activity from one side of the fan to the other are less

frequent when avulsions can occur anywhere on the fan surface. Floodplain sediment can accumulate on the side of the fan opposite channel activity, and these deposits are thick enough to become preserved in the stratigraphy and are less likely to be eroded by the shallower scour depths of ~ 0.15 m

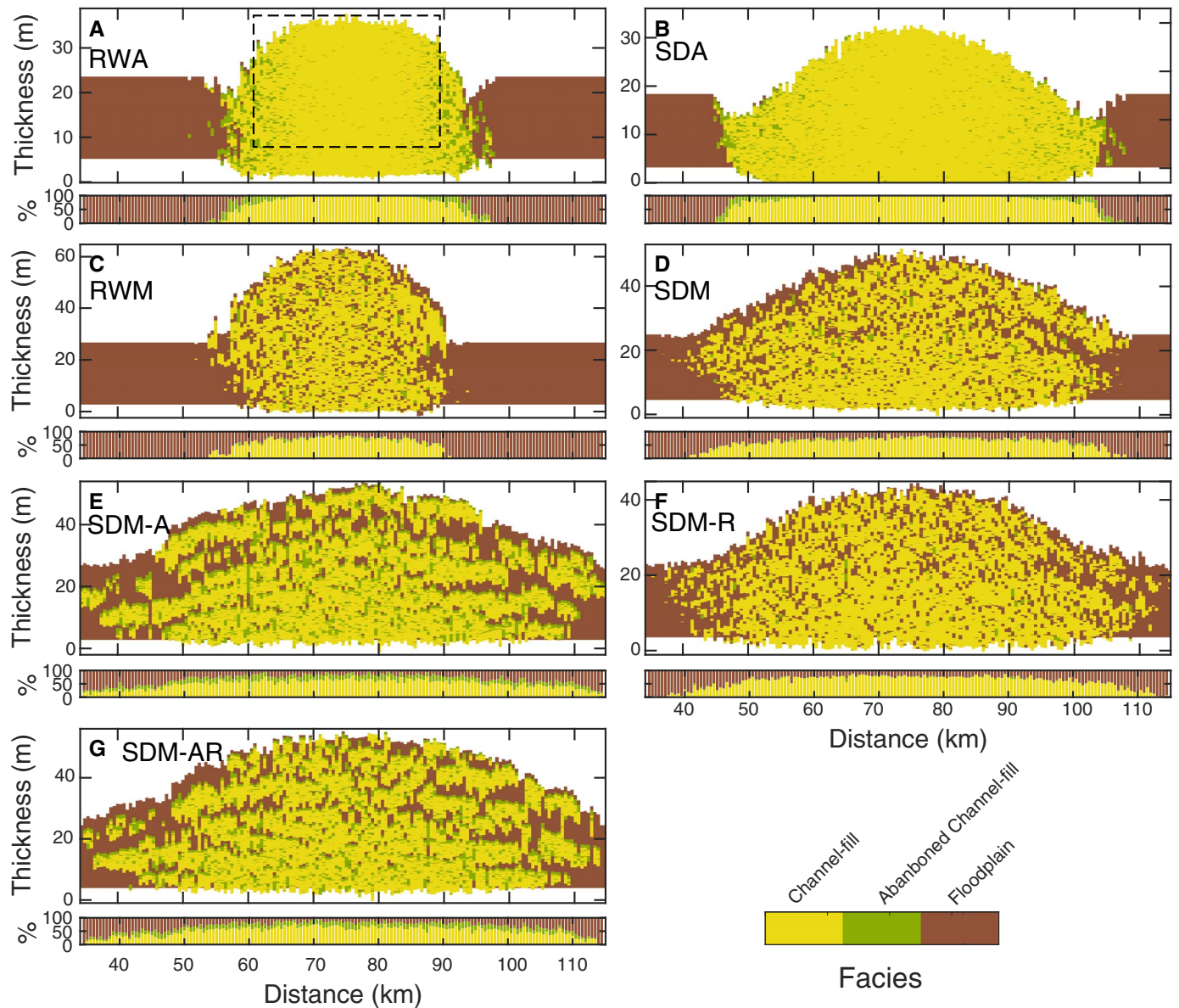


FIG. 3.—A–G) Stratigraphy of each model run at the $\chi = 50\%$ cross section. The colors represent the facies or cell type when deposition occurred. Each stratigraphic cell is 10 cm thick. Immediately below each stratigraphic section shows the facies percentage per column. Distance is cropped to the widest active fan width. The flanking floodplain deposits in Parts A–D are also present in Parts E–F, but they are outside of window shown here. Dashed box in Part A depicts extent of deposit used for compensation analysis in Figure 5.

(Table 1; Fig. 3C, D). In runs SDM-A, SDM-R, and SDM-AR with attraction and repulsion effects, this oscillation and the associated floodplain accumulation become even more pronounced (Fig. 2E–G, 3E–G). This is because the partitioning of the surface creates stronger topographic steering that further limits the occurrence of apical avulsions, increases channel return time, creates both repulsive and attractive obstacles to cross-fan pathfinding, and subsequently creates persistent floodplain deposits that are undisturbed by channels for long periods of time (Table 1). In the case of SDM-AR, floodplain lenses on the sides of the fan have typical thicknesses of ~ 10 m (more than four times the channel depth). Overall, increasing the complexity of pathfinding increases the amount of floodplain facies and decreases the channel fraction to 0.65 (Table 1).

All runs except RWA and SDA have channel activity oscillating from side to side (Fig. 2). Wavelet analysis of channel position through time reveals the

timescale of the oscillations (Table 1; Fig. 4). These oscillations are related to lobe-switching events on the fan surface. For runs RWA and SDA, there is no dominant frequency of lobe switching and wavelet power is spread across all wavelengths. When the condition of only apical avulsions is relaxed, lobe switching emerges and there is a peak in relative wave power (Fig. 4). The timescale of switching is not obviously sensitive to pathfinding rules—the timescale ranges from 42,000 to 415,000 years (Table 1)—nor is it clear why model run SDM-R has the fastest lobe switching timescale of $\sim 42,000$ yr.

Compensation Statistics, Relief Dynamics, and Completeness

Analyses of the sedimentation rates over the middle 25 km of the domain at progressively larger time windows shows that all runs achieve compensation, and the compensational timescale gets longer as the rules for pathfinding become more complex (Table 1, Fig. 5). In the simple runs

TABLE 1.—Model run results. Compensation time is the timescale of slope change marked by the vertical red dashed line in Figure 5A–G. Loss of temporal correlation is the e -folding time of the correlation coefficient in Figure 9. Channel return time is the average time elapsed from abandonment to reoccupation at a given x position and is averaged for all position across the middle 25 km of the domain that is depicted in Figure 3A and also Figure 5H–N. Local relief is the average value of the time series in Figure 6. Long-term aggradation rate is the average deposit thickness over the middle 25 km of the domain divided by elapsed time. Burial timescale is the local relief divided by long-term aggradation rate. Lobe-switching timescale is the peak frequency in Figure 4. Completeness timescale is the time window at which the deposits become 99% complete averaged over the middle 25 km of the domain. Channel deposit fraction is the fraction of the middle 25 km of the domain that is channel fill. Scour depth is the average of all erosion events through space and time across the middle 25 km of the domain.

Run Name	RWA	SDA	RWM	SDM	SDM-A	SDM-R	SDM-AR
	Random-walk pathfinding and apical avulsions	Slope-dependent pathfinding and apical avulsions	Random-walk pathfinding and avulsions anywhere	Slope-dependent pathfinding and avulsions anywhere	Same as SDM with addition of abandoned-channel attraction	Same as SDM with addition of abandoned-channel repulsion	Same as SDM with both attraction and repulsion
Run description							
Compensation time (kyr)	1.72	2.4	15.5	52.7	124.8	52.8	147.3
Loss of temp. corr. (kyr)	1.60	2.82	59.5	45.0	92.8	64.0	81.7
Channel return time (kyr)	2.76	1.79	50.2	56.4	21.5	77.5	20.5
Local relief (m)	1.81 ± 0.27	1.83 ± 0.30	3.29 ± 0.67	2.45 ± 0.36	2.17 ± 0.60	2.29 ± 0.32	2.28 ± 0.60
Long-term aggradation rate (mm/yr)	0.0104	0.00961	0.0193	0.0152	0.0165	0.0134	0.0168
Burial timescale (kyr)	173	190	171	161	132	171	136
Lobe switching timescale (kyr)	—	—	387	337	415	42.1	255
Completeness timescale (kyr)	96.1	117	230	210	228	229	259
Channel deposit fraction	0.96	0.99	0.72	0.74	0.64	0.77	0.65
Average scour depth (m)	0.46	0.42	0.14	0.16	0.13	0.15	0.12

RWA and SDA, compensation is achieved in 1.7 to 2.4 kyr (slope break in Fig. 5), which is orders of magnitude faster than the ~ 170 kyr burial timescale for these runs (mean channel depth divided by long-term aggradation rate; see Table 1). The long-term averaged accumulation rates vary based on the shape of the fan produced with each set of model rules (e.g., narrower, more mounded fan cross sections yield higher cross-section-averaged sedimentation rates than more distributed fans with less mounding and deposition more broadly distributed across the model domains).

When the apical avulsion condition is relaxed, the compensation timescale becomes ~ 15 and 50 kyr for RWM and SDM, respectively (Table 1, Fig. 5), still significantly shorter than the burial timescale. When the rules for attraction and repulsion are added in runs SDM-A, SDM-R, and SDM-AR, the compensation timescale grows to ~ 125 kyr, closer to the burial timescale (Table 1, Fig. 5). While all runs show a transition from low ($\kappa \sim 0.5$ – 0.6) to high ($\kappa \geq 0.8$) compensation index values, the more complex runs (SDM-A, SDM-R, SDM-AR) have a long-term compensation index close to 1, and

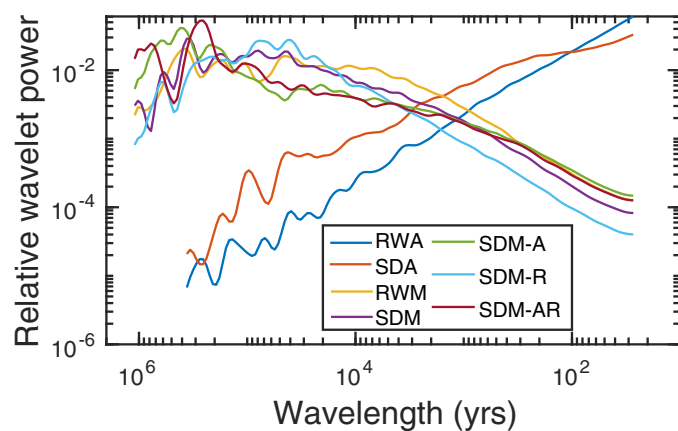


FIG. 4.—Time-integrated wavelet analysis of the channel position shown in Figure 2. Relative wavelet power is scaled by the total power for all wavelengths. Notice that there are peaks in relative wavelet power in all runs except RWA and SDA, indicating that there is a dominant frequency of channel switching.

the simpler runs do not all reach full compensation (Fig. 5). The simpler runs also show a trend toward increasing topographic relief through time, whereas the more complex runs show stable, albeit variable, topographic relief through time (Fig. 6). Long-term trends toward increasing relief and the possibility of progressive (rather than sharp) transitions between short-term variability to long-term basin filling trends can contribute to sub-compensational long-term values (Trampush et al. 2017).

The topographic memory of each run changes with pathfinding rules. We calculated the autocorrelation timescales for each relief series in Figure 6 by determining the lag time (or shift) at which the autocorrelation coefficient reduced by a factor of $1/e$ (Fig. 7). The choice of $1/e$ is sensible because the function shows an approximately exponential decay. At lag time of 0 the correlation coefficient is 1 because the signal perfectly correlates with itself, and at larger lag times the correlation decreases because the lagged signal becomes dissimilar to the original. In some cases, the autocorrelation function has a sharp and narrow peak, indicating rapid loss in correlation (Fig. 7A, B), whereas in other cases the function is wider, indicating a slower loss (Fig. 7E). The time it takes to lose correlation indicates the topographic memory; the memory is short for RWA and SDA and longer as pathfinding complexity increases (Table 1).

Stratigraphic completeness also changes as a function of pathfinding rules. For a given time span, completeness is the percentage of surfaces that resulted in preserved deposition. There are two notable effects. First, at short time spans (duration < 1000 yr), more complex runs (SDM-A, SDA-R, SDA-AR) are an order of magnitude more complete than simpler runs (RWA, SDA) (Fig. 8). Second, 99% completeness is reached at a later duration for the more complex runs than for the simple runs (Table 1, Fig. 8).

Increasing complexity of pathfinding rules causes increases in the compensational timescale, lobe-switching timescale, the completeness timescale, and the timescale of correlation loss of surface roughness (Fig. 9A–C). The burial timescales for all runs range from ~ 130 to 190 kyr and seems to decrease with increasing model complexity. The burial timescale is consistently long regardless of pathfinding complexity because it is set by the long-term aggradation rate and the local relief. Previous work suggests that the burial timescale should be roughly the same as the compensation timescale (Hajek and Straub 2017). Our model results show a

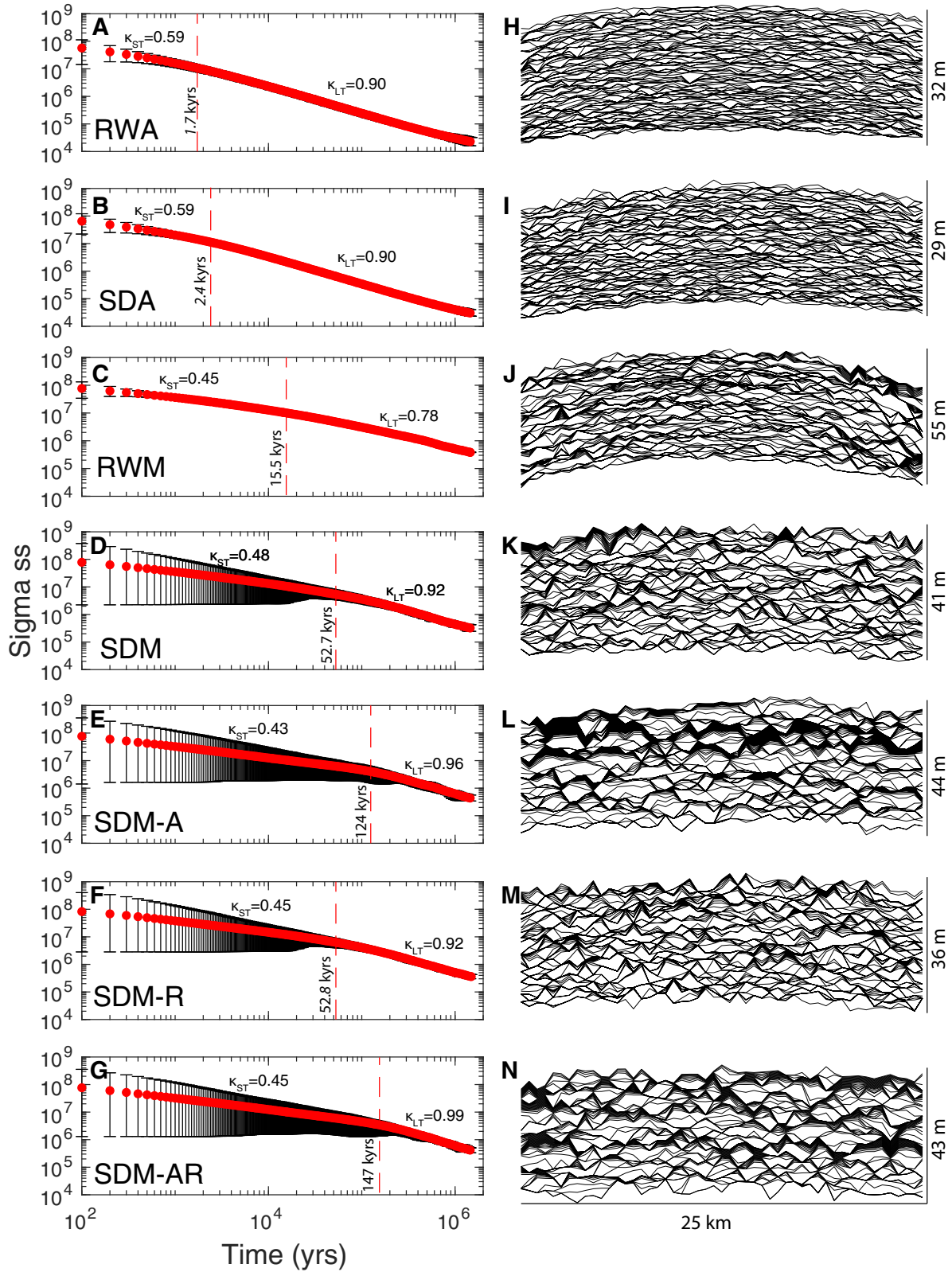


FIG. 5.—Compensation plots (Parts A–G) calculated for each corresponding series of stratigraphic surfaces (Parts H–N). Stratigraphic surfaces are clipped for erosion and show model output at the $\chi = 50\%$ cross section. Surfaces span the time from 1 Myr to 3 Myr to avoid spin-up associated with fan growth and the establishment of lobe switching. The span of the stratigraphy corresponds to the dashed box in Figure 3A. The stratigraphy shows one surface every 3000 yr, but the full stack of surfaces (one every 10 yr) was used for statistics in Parts A–G. The dashed red line shows the position of the slope break that marks the compensational timescale. κ_{ST} and κ_{LT} are those slopes of the points before and after the red line, respectively. The error bars show geometric standard deviation.

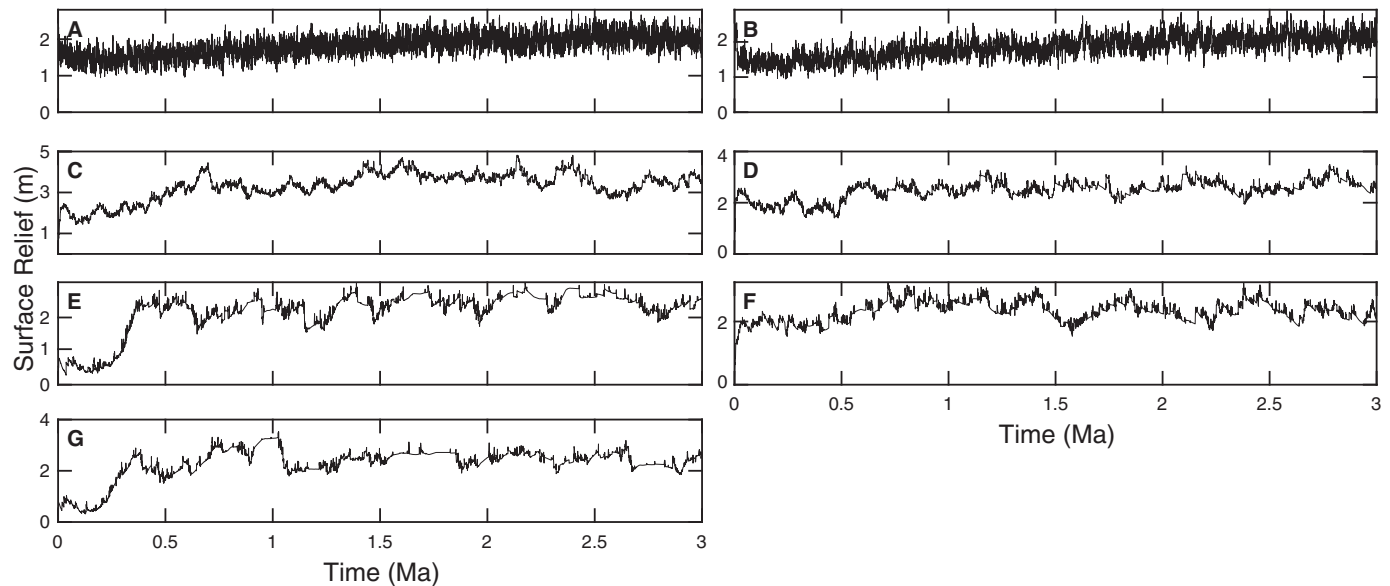


FIG. 6.—Surface relief through time for each model run (Parts A–G). Relief is calculated as the spatially averaged elevation difference within a three-cell moving window along the $\chi = 50\%$ cross sections shown in Figure 5H–N. This is calculated over the middle 25 km of the domain as shown by the dashed box in Figure 3A.

significant (several orders of magnitude) offset between the burial timescale and the compensation timescale for the simplest model runs (Fig. 9D).

DISCUSSION

Pathfinding Complexity Drives Changes in Stratigraphic Architecture

As the rules for pathfinding increase in complexity there are substantive and important changes to the resulting stratigraphy and architecture, even without changes in allogenic forcings. An increase in pathfinding complexity creates: 1) more organized channel movement (Fig. 2) with well-defined lobe switching events (Fig. 4); 2) more stratigraphic variability with preserved packages of floodplain deposition and lower overall channel fraction (Table 1, Fig. 3); 3) longer compensational timescales (Fig. 5); 4) more complete stratigraphy at short timescales (Fig. 8); and 5) longer timescales associated with total completeness (Fig. 8).

These changes arise because adding more rules for pathfinding creates additional scales within the fluvial process hierarchy (*sensu* Ganti et al. 2020). The simplest possible rule for pathfinding (RWA) results in a system with little memory and with rapid channel switching with an average return time to a given location of 2.7 kyr (Table 1). The mobile channel rapidly reworks the surface, preserving only channel-fill deposits (Fig. 3) and reducing stratigraphic completeness over short timescales (Fig. 8). After all, for RWA and SDA, the average scour depth is nearly three times greater than in all other runs (Table 1). But in real systems, channels on fans are subject to more than just random walk; adding more pathfinding rules, like attraction and repulsion, creates more complex spatio-temporal avulsion patterns from which larger-scale organization arises, creating a morphodynamic hierarchy where, for example, shorter channel avulsions are embedded within a larger and longer timescale structure of lobe switching across the fan. With the emergence of lobe switching, the average channel return time increases to ~ 50 kyr because roughly half of the fan can become abandoned by channels at a given time. On the abandoned side of the fan, floodplain packages are deposited and preserved (Fig. 3) and stratigraphic completeness goes up (Fig. 8) because, in the absence of channels, long successions of floodplain deposition accumulate without interruption.

Why is the Compensation Timescale Detached from the Burial Timescale?

Over the last 15 years the prevailing thought has been that the structure of stratigraphic fills in sedimentary basins matches the external forcing at the burial timescale (Straub et al. 2009; Hajek and Straub 2017). Our results show that the burial timescale is relatively consistent (it varies by 60 kyr) for all runs, whereas the compensational timescale increases with complexity (Fig. 9D, Table 1). We were surprised to find compensational deposition across all runs, especially in simple runs RWA and SDA that have random pathfinding processes. After all, in simple cross-sectional models that randomly emplace channel bodies, the stratigraphy is stochastic across all time windows (Straub et al. 2009). Instead, our simple runs with random channel emplacement show compensation but at timescales much shorter than the burial timescales (Table 1). This occurs because the surface relief exhibits random variability with minimal temporal correlation (Table 1, Fig. 7A, B). Subtracting each measurement from the next (lag-1 differences) in such random processes results in differences that alternate in sign, creating anticorrelation. Thus, fast compensation occurs in these runs because if sedimentation rate (or topography) is randomly low on one time step, statistically it will likely be higher (or aggrade) during the next reoccupation. This alteration in deposition rates from slow to fast (or fast to slow) is the hallmark of topographic compensation as it pushes a system toward its long-term deposition rate (Mutti and Sonnino 1981; Deptuck et al. 2008; Straub et al. 2009). This effect did not show up in the simple 1-D cross-sectional models (Straub et al. 2009) because in those cases random channel visitation was prescribed to cause deposition. In our model, random visitation (runs RWA and SDA) does not result in just random deposition; rather, deposition (or erosion) is nonrandom and determined by diffusion of the longitudinal profile down the channel centerline.

In fact, we find that runs achieve compensation when temporal correlation of the surface roughness is lost (Fig. 9C). The burial timescale is a good approximation of the compensation timescale in our experiments only when the temporal correlation in surface topography is long because the long correlation in surface processes creates local topographic roughening that is later compensated for during lobe switching. This occurs in the more complex runs (SDM-A and SDM-

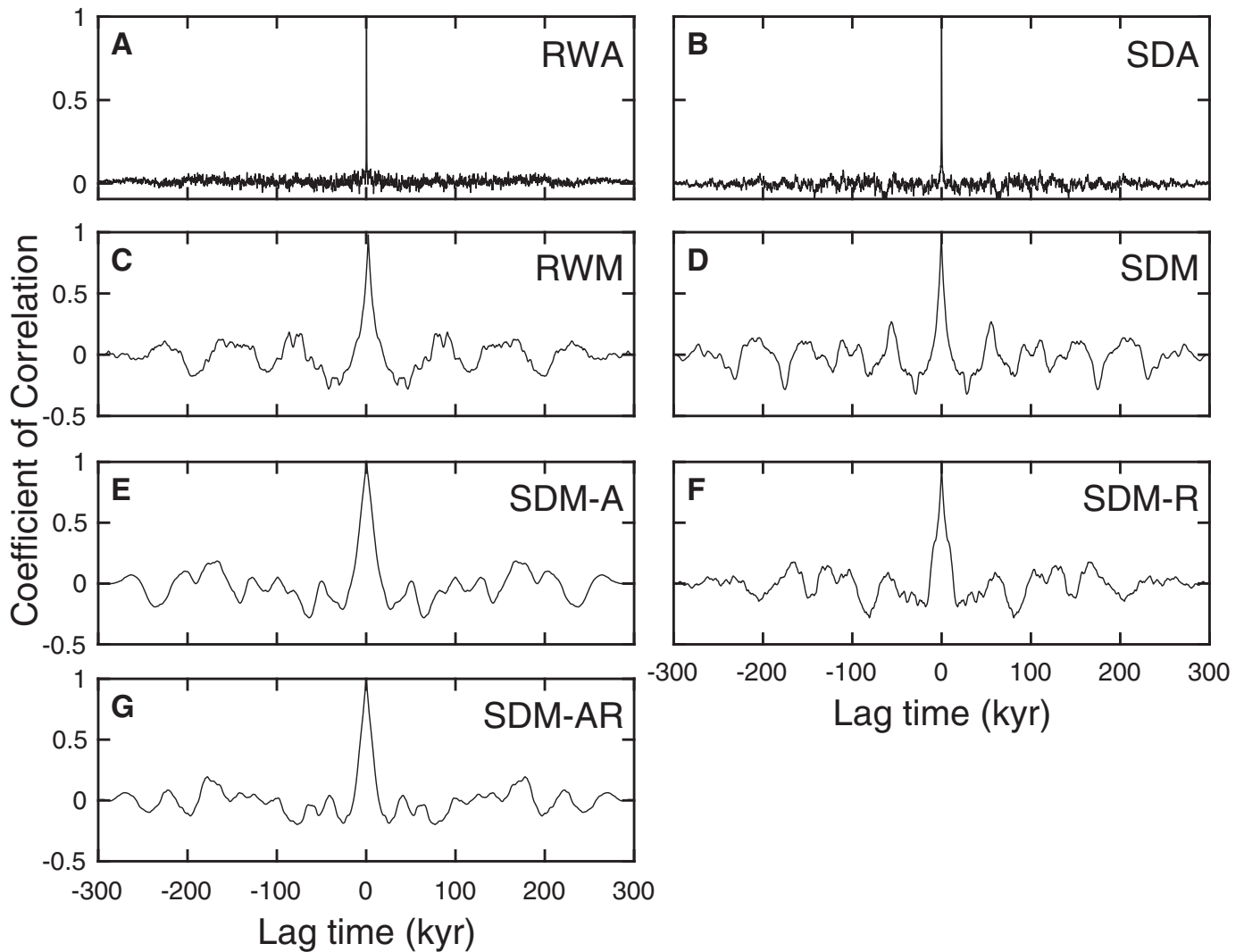


FIG. 7.—Autocorrelation of the relief variability through time shown in Figure 5. The y axis is the correlation coefficient of the autocorrelation analysis.

AR, Table 1) and in physical fan delta experiments (Straub and Wang 2013). The long temporal correlation in surface topography likely reflects most natural alluvial-basin conditions where basins are not overfilled with sediment. In these settings, surfaces can subside more than one relief length scale below the mean topography and then flow and sediment are attracted into that location. In our simple model runs, however, the basin is overfilled (i.e., substantial positive topography is built; Fig. 3), and this prevents local roughening due to subsidence and attraction into topographic lows (i.e., minimizes temporal correlation of surfaces). The complex runs are also overfilled, but the lobe switching that emerges abandons sections of the fan and establishes this temporal correlation. The importance of temporal correlation may have gone unnoticed because in most physical experiments the sediment-transporting system is unconstrained and struggles to fill accommodation space (e.g., Straub et al. 2023).

Applying These Results to Natural Systems

The more complex runs (SDM-A, SDM-AR) behave like we expect for fluvial or alluvial fans. There is a clear correspondence between the burial and compensation timescales, consistent with previous work (e.g., Hajek

and Straub 2017). It is not immediately clear, however, what the best analogy is for the simple runs. In the simple runs with no attraction and repulsion (RWA, SDA, RWM, SDM), the burial and compensation timescales are detached because the time series of surface roughness has minimal correlation (Fig. 7, Table 1). We suspect that this could occur in natural systems where the channel rapidly moves around the surface, ignoring pre-existing topography, and creating a system with little memory. This scenario might be limited to cases where extreme width restriction and/or significant flow variability drive channel movements and sedimentation patterns, superseding the role of preexisting topography in driving channel relocation (Lunt et al. 2013; Greenberg et al. 2023). Just as we might expect for an incised valley where channels are confined by relatively narrow valleys, the pathfinding rules in our simple models force the channel to stay in the center of the model domain, effectively restricting lateral channel avulsion pathways (Blum and Aslan 2006). Another possibility is that this might arise in canyon-fan systems near the alluvial-fan apex. At this position, channel return time is fast because avulsions are routed over a smaller area (Owen et al. 2015; Chamberlin and Hajek 2019). Short avulsion return times and a lack of topographic memory may manifest as poor preservation (i.e., significant reworking) of channel and bar deposits in field-scale systems (Chamberlin and Hajek

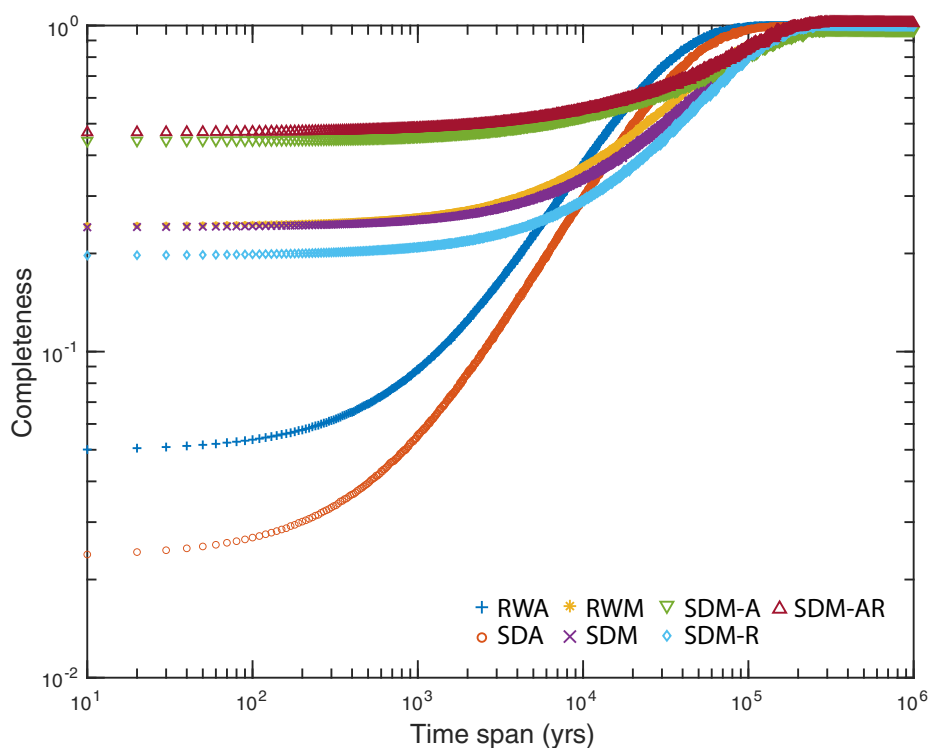


FIG. 8.—Stratigraphic completeness for each model run. Completeness, for a given time span, is the fraction of time recorded in the strata relative to the total elapsed time across the width of the fan shown in Figure 3H–N.

2019). This causes the rapid loss of topographic correlation and a system with little memory that creates an even basin fill at short timescales but with low stratigraphic completeness due to surface reworking.

Our results also suggest that the compensation timescale lengthens as a function of complexity and the emergence of a morphodynamic hierarchy. These runs show compensation occurs from 2 to 150 kyr. This range of timescale overlaps significantly with the common range of allogenic forcing, such as Milankovitch-scale climatic forcing ranging from 20 to 400 kyr (Romans et al. 2016). This in turn suggests that when we view compensation through the lens of losing temporal correlation the large range of timescales that emerges may complicate untangling autogenic and allogenic signals.

CONCLUSIONS

Here we use a rule-based model of a fluvial fan to simulate how the stratigraphic architecture changes as rules for avulsion channel pathfinding become more complex. The simplest models assumed that all avulsions occurred at the fan apex and that pathfinding was determined by random walk or slope-dependent random walk. Then runs became progressively more complex by relaxing the apical avulsion condition and allowing avulsions anywhere on the fan surface, and then allowing abandoned channels on the fan to attract or repel advancing avulsion channels. As the complexity of avulsion pathfinding rules increases, the channel dynamics and stratigraphic architecture change significantly. Firstly, channel movement across the fan surface becomes more organized with well-defined lobe switching events. Secondly, stratigraphic variability increases, resulting in the preservation of distinct packages of floodplain deposits and a reduction in the overall fraction of channels within the system. Thirdly, the compensational timescale lengthens, indicating a lengthening of the period over which sedimentary systems adjust to perturbations, thereby influencing the temporal

evolution of stratigraphy. Finally, the stratigraphy becomes more complete, especially at short timescales.

These observed changes in stratigraphic architecture are attributed to the emergence of additional scales within the fluvial process hierarchy of sedimentary systems, whereby the introduction of more complex pathfinding rules gives rise to larger-scale organization within the system, with shorter channel avulsions becoming embedded within broader, longer-term structures of lobe switching across the fan. Consequently, the average channel return time increases substantially, reflecting the propensity for channels to abandon and reoccupy portions of the fan surface. On the abandoned sectors, the deposition and preservation of floodplain packages contribute to enhanced stratigraphic completeness, as uninterrupted sequences of sediment accumulation ensue in the absence of active channels.

Our study suggests that in simple models the burial and compensational timescale are detached. This occurs because the burial timescale is relatively consistent among runs; it is set by average surface relief relative to long-term aggradation. The compensational timescale is related to the loss of temporal correlation of surface roughness because this determines the influence of topography on channel dynamics and hence compensation. The compensation and loss of surface roughness is fast in simple runs because the minimal pathfinding rules create mobile channels that rapidly smooth the surface with deposition. Overall, our findings underscore the pivotal role of pathfinding complexity in shaping the stratigraphic architecture of sedimentary systems and provide valuable insights into the interplay between surface processes and stratigraphic evolution.

ACKNOWLEDGMENTS

DAE, CS, and HKM were funded by National Science Foundation (NSF) grants 1911321 and 2321056. HKM was supported by National Aeronautics and Space Administration (NASA) Future Investigators in NASA Earth and Space Science and Technology (FINESST) grant 80NSSC21K1598. EAH contributions were supported by NSF 1935513. Model code for RiverWalk with

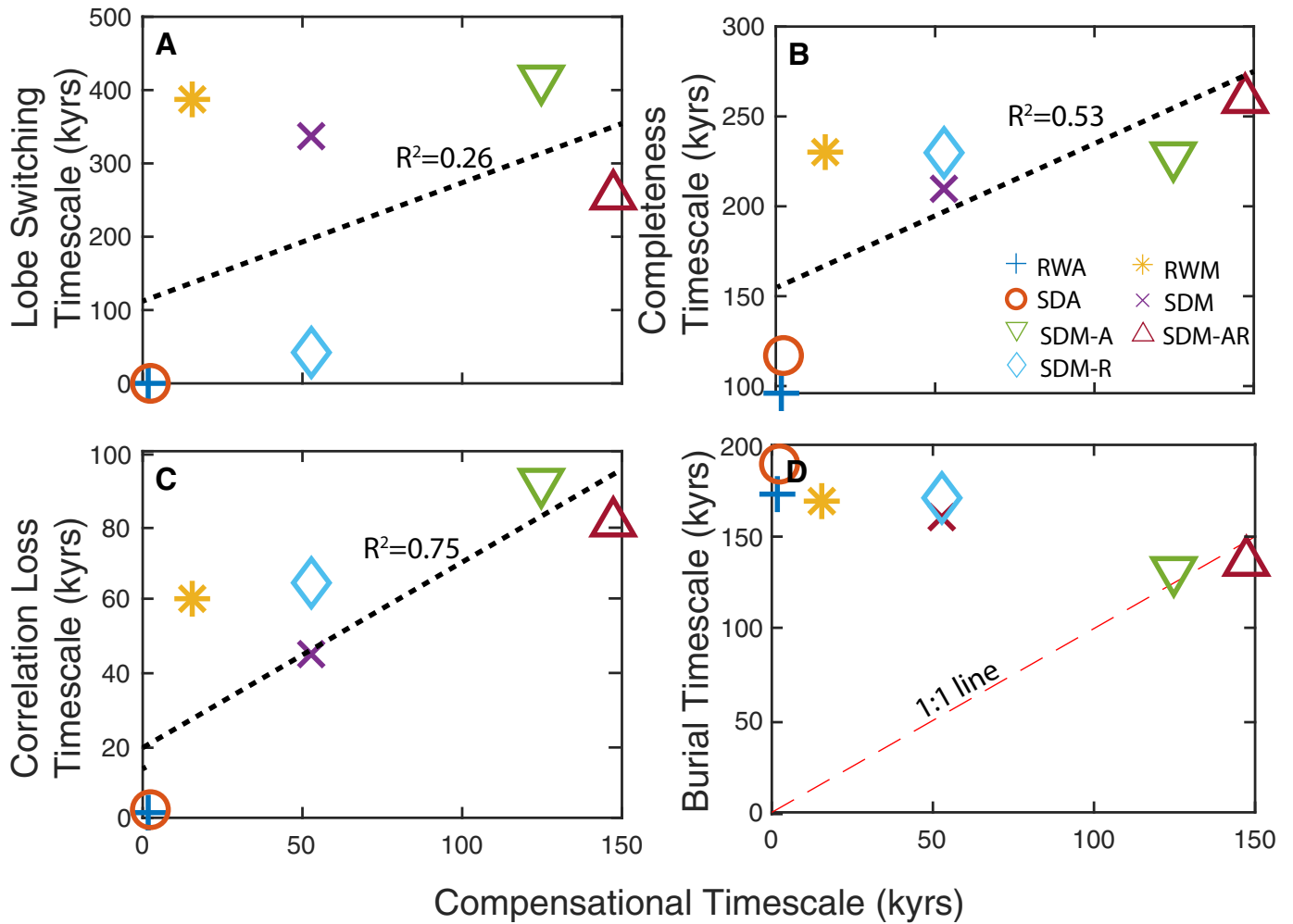


FIG. 9.—**A–D**) Linear correlations between the compensational timescale and other timescales measured in the experiments. All timescales are described and reported in Table 1.

the stratigraphic module (RiverWalk-Strat) is available at <https://github.com/harrison-martin/RiverWalk-Strat>. We thank C. Broadus for discussion and Associate Editor V. Ganti, reviewer Y. Wang, and an anonymous reviewer whose comments improved this manuscript.

REFERENCES

- ALLEN, J.R.L., 1978, Studies in fluvial sedimentation: an exploratory quantitative model for the architecture of avulsion-controlled alluvial suites: *Sedimentary Geology*, v. 21, p. 129–147.
- ASSINE, M.L., 2005, River avulsions on the Taquari megafan, Pantanal wetland, Brazil: *Geomorphology*, v. 70, p. 357–371.
- BERNAL, C., CHRISTOPHOUL, F., DARROZES, J., SOULA, J.-C., BABY, P., AND BURGOS, J., 2011, Late Glacial and Holocene avulsions of the Rio Pastaza Megafan Ecuador–Peru: frequency and controlling factors: *International Journal of Earth Sciences*, v. 100, p. 1759–1782.
- BLUM, M.D., AND ASLAN, A., 2006, Signatures of climate vs. sea-level change within incised valley-fill successions: Quaternary examples from the Texas Gulf Coast: *Sedimentary Geology*, v. 190, p. 177–211.
- BRIDGE, J.S., AND LEEDER, M.R., 1979, A simulation model of alluvial stratigraphy: *Sedimentology*, v. 26, p. 617–644.
- CHAKRABORTY, T., KAR, R., GHOSH, P., AND BASU, S., 2010, Kosi megafan: historical records, geomorphology and the recent avulsion of the Kosi River: *Quaternary International*, v. 227, p. 143–160.
- CHAMBERLIN, E.P., AND HAJEK, E.A., 2015, Interpreting paleo-avulsion dynamics from multistory sand bodies: *Journal of Sedimentary Research*, v. 85, p. 82–94.
- CHAMBERLIN, E.P., AND HAJEK, E.A., 2019, Using bar preservation to constrain reworking in channel-dominated fluvial stratigraphy: *Geology*, v. 47, p. 531–534.
- CHAMBERLIN, E.P., HAJEK, E.A., AND TRAMPUSH, S.M., 2016, measuring scales of autogenic organization in fluvial stratigraphy: an example from the Cretaceous Lower Williams Fork Formation, Colorado, in Budd, D.A., Hajek, E.A., and Purkis, S.J., eds., *Autogenic Dynamics and Self-Organization in Sedimentary Systems*: SEPM, Special Publication 106, p. 132–144.
- DEPTUCK, M.E., PIPER, D.J.W., SAVOYE, B., AND GERVAIS, A., 2008, Dimensions and architecture of late Pleistocene submarine lobes off the northern margin of East Corsica: *Sedimentology*, v. 55, p. 869–898.
- FOREMAN, B.Z., AND STRAUB, K.M., 2017, Autogenic geomorphic processes determine the resolution and fidelity of terrestrial paleoclimate records: *Science Advances*, v. 3, no. e1700683.
- GANTI, V., HAJEK, E.A., LEARY, K., STRAUB, K.M., AND PAOLA, C., 2020, Morphodynamic hierarchy and the fabric of the sedimentary record: *Geophysical Research Letters*, v. 47, e2020GL087921.
- GEARON, J.H., MARTIN, H.K., DELISLE, C., BAREDFOOT, E.A., MOHRIG, D., PAOLA, C., AND EDMONDS, D.A., 2024, Rules of river avulsion change downstream: *Nature*, v. 634, p. 91–95.
- GREENBERG, E., CHADWICK, A.J., AND GANTI, V., 2023, A generalized area-based framework to quantify river mobility from remotely sensed imagery: *Journal of Geophysical Research, Earth Surface*, v. 128, no. e2023JF007189.
- HAJEK, E.A., AND STRAUB, K.M., 2017, Autogenic sedimentation in clastic stratigraphy: *Annual Review of Earth and Planetary Sciences*, v. 45, p. 681–709.
- HANSFORD, M.R., AND PLINK-BJÖRKLUND, P., 2020, River discharge variability as the link between climate and fluvial fan formation: *Geology*, v. 48, p. 952–956.
- HARIHARAN, J., PASSALACQUA, P., XU, Z., MICHAEL, H.A., STEEL, E., CHADWICK, A., PAOLA, C., AND MOODIE, A.J., 2022, Modeling the dynamic response of river deltas to sea-level rise acceleration: *Journal of Geophysical Research, Earth Surface*, v. 127, no. e2022JF006762.
- JEROLMACK, D.J., AND PAOLA, C., 2007, Complexity in a cellular model of river avulsion: *Geomorphology*, v. 91, p. 259–270.

- KARSSENBERG, D., AND BRIDGE, J.S., 2008, A three-dimensional numerical model of sediment transport, erosion and deposition within a network of channel belts, floodplain and hill slope: extrinsic and intrinsic controls on floodplain dynamics and alluvial architecture: *Sedimentology*, v. 55, p. 1717–1745.
- KEMP, D.B., 2012, Stochastic and deterministic controls on stratigraphic completeness and fidelity: *International Journal of Earth Science*, v. 101, p. 2225–2238.
- KUMAR, P., AND FOUFOULA-GEORGIU, E., 1997, Wavelet analysis for geophysical applications: *Reviews in Geophysics*, v. 35, p. 385–412.
- LEIER, A.L., DECELLES, P.G., AND PELLETIER, J.D., 2005, Mountains, monsoons, and megafans: *Geology*, v. 33, p. 289–292.
- LI, Q., YU, L., AND STRAUB, K.M., 2016, Storage thresholds for relative sea-level signals in the stratigraphic record: *Geology*, v. 44, p. 179–182.
- LI, Q., BENSON, M.W., HARLAN, M., ROBICHAUX, P., SHA, X., XU, K., AND STRAUB, K.M., 2017, Influence of sediment cohesion on deltaic morphodynamics and stratigraphy over basin-filling time scales: *Journal of Geophysical Research, Earth Surface*, v. 122, p. 1808–1826.
- LI, Z., WANG, H., NITTROUER, J.A., BI, N., WU, X., AND CARLSON, B., 2020, Modeling the infilling process of an abandoned fluvial-deltaic distributary channel: an example from the Yellow River delta, China: *Geomorphology*, v. 361, no. 107204.
- LUNT, I.A., SAMBROOK SMITH, G.H., BEST, J.L., ASHWORTH, P.J., LANE, S.N., AND SIMPSON, C.J., 2013, Deposits of the sandy braided South Saskatchewan River: implications for the use of modern analogs in reconstructing channel dimensions in reservoir characterization: *American Association of Petroleum Geologists, Bulletin*, v. 97, p. 553–576.
- MACKAY, S.D., AND BRIDGE, J.S., 1995, Three-dimensional model of alluvial stratigraphy: theory and applications: *Journal of Sedimentary Research*, v. 65, p. 7–31.
- MARTIN, H.K., AND EDMONDS, D.A., 2022, The push and pull of abandoned channels: how floodplain processes and healing affect avulsion dynamics and alluvial landscape evolution in foreland basins: *Earth Surface Dynamics*, v. 10, p. 555–579.
- MARTIN, H.K., AND EDMONDS, D.A., 2023, Avulsion dynamics determine fluvial fan morphology in a cellular model: *Geology*, v. 51, p. 796–800.
- MORAN, K.E., NITTROUER, J.A., PERILLO, M.M., LORENZO-TRUEBA, J., AND ANDERSON, J.B., 2017, Morphodynamic modeling of fluvial channel fill and avulsion time scales during early Holocene transgression, as substantiated by the incised valley stratigraphy of the Trinity River, Texas: *Journal of Geophysical Research, Earth Surface*, v. 122, p. 215–234.
- MUTTHI, E., AND SONNINO, M., 1981, Compensation cycles: a diagnostic feature of turbidite sandstone lobes [Abstract]: *Bologna, International Association of Sedimentologists, 2nd European Meeting*, p. 120–123.
- OWEN, A., NICHOLS, G.J., HARTLEY, A.J., WEISSMANN, G.S., AND SCUDERI, L.A., 2015, Quantification of a distributive fluvial system: the Salt Wash DFS of the Morrison Formation, SW USA: *Journal of Sedimentary Research*, v. 85, p. 544–561.
- PAOLA, C., AND MARTIN, J.M., 2012, Mass-balance effects in depositional systems: *Journal of Sedimentary Research*, v. 82, p. 435–450.
- PAOLA, C., HELLER, P.L., AND ANGEVINE, C.L., 1992, The large-scale dynamics of grain-size variation in alluvial basins, 1: theory: *Basin Research*, v. 4, p. 73–90.
- REITZ, M.D., AND JEROLMACK, D.J., 2012, Experimental alluvial fan evolution: channel dynamics, slope controls, and shoreline growth: *Journal of Geophysical Research*, v. 117, F02021.
- REITZ, M., JEROLMACK, D., AND SWENSON, J., 2010, Flooding and flow path selection on alluvial fans and deltas: *Geophysical Research Letters*, v. 37, no. L06401.
- ROMANS, B.W., CASTELLTORT, S., COVAULT, J.A., FILDANI, A., AND WALSH, J., 2016, Environmental signal propagation in sedimentary systems across timescales: *Earth-Science Reviews*, v. 153, p. 7–29.
- ROSSETTI, D.F., AND VALERIANO, M.M., 2007, Evolution of the lowest amazon basin modeled from the integration of geological and SRTM topographic data: *Catena*, v. 70, p. 253–265.
- SADLER, P.M., 1981, Sediment accumulation rates and the completeness of stratigraphic section: *Journal of Geology*, v. 89, p. 569–584.
- SADLER, P.M., 1993, Models of time-averaging as a maturation process: How soon do sedimentary sections escape reworking?: *Cambridge University Press, Short Courses in Paleontology*, v. 6, p. 188–209.
- SALTER, G., VOLLER, V.R., AND PAOLA, C., 2020, Chaos in a simple model of a delta network: *National Academy of Sciences [USA], Proceedings*, v. 117, p. 27,179–27,187.
- SHEETS, B.A., HICKSON, T.A., AND PAOLA, C., 2002, Assembling the stratigraphic record: depositional patterns and time-scales in an experimental alluvial basin: *Basin Research*, v. 14, p. 287–301.
- STANISTREET, I.G., AND MCCARTHY, T.S., 1993, The Okavango Fan and the classification of subaerial fan systems: *Sedimentary Geology*, v. 85, p. 115–133.
- STRAUB, K.M., AND FOREMAN, B.Z., 2018, Geomorphic stasis and spatiotemporal scales of stratigraphic completeness: *Geology*, v. 46, p. 311–314.
- STRAUB, K.M., AND PYLES, D.R., 2012, Quantifying the hierarchical organization of compensation in submarine fans using surface statistics: *Journal of Sedimentary Research*, v. 82, p. 889–898.
- STRAUB, K.M., AND WANG, Y., 2013, Influence of water and sediment supply on the long-term evolution of alluvial fans and deltas: statistical characterization of basin-filling sedimentation patterns: *Journal of Geophysical Research, Earth Surface*, v. 118, p. 1602–1616.
- STRAUB, K.M., PAOLA, C., MOHRIG, D., WOLINSKY, M.A., AND GEORGE, T., 2009, Compensational stacking of channelized sedimentary deposits: *Journal of Sedimentary Research*, v. 79, p. 673–688.
- STRAUB, K.M., LI, Q., AND BENSON, W.M., 2015, Influence of sediment cohesion on deltaic shoreline dynamics and bulk sediment retention: a laboratory study: *Geophysical Research Letters*, v. 42, p. 9808–9815.
- STRAUB, K.M., DULLER, R.A., FOREMAN, B.Z., AND HAJEK, E.A., 2020, Buffered, incomplete, and shredded: the challenges of reading an imperfect stratigraphic record: *Journal of Geophysical Research, Earth Surface*, v. 125, no. e2019JF005079.
- STRAUB, K.M., DUTT, R., AND DULLER, R.A., 2023, Coupled channel–floodplain dynamics and resulting stratigraphic architecture viewed through a mass-balance lens: *Journal of Sedimentary Research*, v. 93, p. 595–616.
- TIPPER, J.C., 1983, Rates of sedimentation and stratigraphical completeness: *Nature*, v. 302, p. 696–698.
- TOONEN, W.H.J., KLEINHANS, M.G., AND COHEN, K.M., 2012, Sedimentary architecture of abandoned channel fills: *Earth Surface Processes and Landforms*, v. 37, p. 459–472.
- TRAMPUSH, S.M., HAJEK, E.A., STRAUB, K.M., AND CHAMBERLIN, E.P., 2017, Identifying autogenic sedimentation in fluvial-deltaic stratigraphy: evaluating the effect of outcrop-quality data on the compensation statistic: *Journal of Geophysical Research, Earth Surface*, v. 122, p. 91–113.
- VALENZA, J.M., EDMONDS, D.A., HWANG, T., AND ROY, S., 2020, Downstream changes in river avulsion style are related to channel morphology: *Nature Communications*, v. 11, no. 2116.
- WANG, Y., STRAUB, K.M., AND HAJEK, E.A., 2011, Scale-dependent compensational stacking: an estimate of autogenic time scales in channelized sedimentary deposits: *Geology*, v. 39, p. 811–814.
- WANG, Y., STORMS, J.E.A., MARTINIUS, A.W., KARSSENBERG, D., AND ABELS, H.A., 2021, Evaluating alluvial stratigraphic response to cyclic and non-cyclic upstream forcing through process-based alluvial architecture modelling: *Basin Research*, v. 33, p. 48–65.
- WANG, Y., BAARS, T.F., STORMS, J.E.A., MARTINIUS, A.W., GINGERICH, P.D., CHMIELEWSKA, M., BUCKLEY, S.J., AND ABELS, H.A., 2023, Lateral and vertical characteristics of floodplain aggradation cycles in the lower Eocene Willwood Formation, Bighorn Basin, Wyoming, USA: *Geological Society of America, Bulletin*, v. 136, p. 2568–2581.
- WEISSMANN, G.S., HARTLEY, A.J., SCUDERI, L.A., NICHOLS, G.J., DAVIDSON, S.K., OWEN, A., ATCHLEY, S.C., BHATTACHARYYA, P., CHAKRABORTY, T., GHOSH, P., NORDT, L.C., MICHEL, L., AND TABOR, N.J., 2013, Prograding distributive fluvial systems: geomorphic models and ancient examples, *in* Driese, S.G., Nordt, L.C., and McCarthy, P.L., eds., *New Frontiers in Paleopedology and Terrestrial Paleoclimatology: Paleosols and Soil Surface Analog Systems: SEPM, Special Publication 104*, p. 131–147.

Received 2 April 2024; accepted 6 November 2024.